

Gravimeter Search for Compact Dark Matter Objects Moving in the Earth

C. J. Horowitz^{*}

*Center for Exploration of Energy and Matter and Department of Physics, Indiana University,
Bloomington, Indiana 47405, USA*

R. Widmer-Schmidrig[†]

*Black Forest Observatory (BFO), Heubach 206, D-77709 Wolfach, Germany
and Institute of Geodesy, Stuttgart University, Stuttgart, Germany*

 (Received 13 September 2019; accepted 8 January 2020; published 7 February 2020)

Dark matter could be composed of compact dark objects (CDOs). These objects may interact very weakly with normal matter and could move freely *inside* the Earth. A CDO moving in the inner core of the Earth will have an orbital period near 55 min and produce a time-dependent signal in a gravimeter. Data from superconducting gravimeters rule out such objects moving inside the Earth unless their mass m_D and or orbital radius a are very small so that $m_D a < 1.2 \times 10^{-13} M_\oplus R_\oplus$. Here, M_\oplus and R_\oplus are the mass and radius of the Earth, respectively.

DOI: [10.1103/PhysRevLett.124.051102](https://doi.org/10.1103/PhysRevLett.124.051102)

Many dark matter direct detection experiments have not yet seen a clear signal. Limits from most of these experiments can be avoided if dark matter is concentrated into macroscopic objects. Dark matter, or one component of it, could be composed of compact dark objects (CDOs). These objects are assumed to have small nongravitational interactions with normal matter and could be primordial black holes; see, e.g., Ref. [1]. Some other possibilities or names for CDOs include boson stars [2], dark blobs [3], asymmetric dark matter nuggets [4], exotic compact objects [5], ultracompact minihalos [6] made, for example, of axions [7], and macros [8]. Microlensing observations rule out most of dark matter being made of CDOs with masses between 10^{-11} and $15 M_\odot$ [9–13]. In this Letter, we focus on CDOs with masses between about 10^{-19} and $10^{-11} M_\odot$. We assume the objects are not black holes (to avoid destroying the Earth) but otherwise try to minimize our assumptions about detailed CDO properties.

Dark matter is known to have gravitational interactions. Therefore, it is appealing to search for dark matter using gravity. Compact dark objects can radiate detectable gravitational waves (GWs) [5,14]. The LIGO-Virgo Collaboration searched for GWs from CDO binaries with masses in the range of 0.2 – $1 M_\odot$ [15]. We explored GW signals from CDOs merging with neutron stars [16]. In addition, we searched for GWs from CDOs orbiting inside the Sun [17] and ruled out close binaries with masses above $10^{-9} M_\odot$.

To probe CDO masses well below $10^{-9} M_\odot$, we now consider CDOs moving around or *inside* the Earth. It can be difficult to constrain such low mass objects with microlensing [9] or femtolensing [18] because of the small size of the lens compared to the background star or gamma ray

burst. Instead, nearby CDOs could produce detectable signals in gravimeters [19] that measure the local acceleration due to gravity.

Sensitive superconducting gravimeters have been deployed at several locations around the world [20]. They are used to observe a wide range of geophysical phenomena including the Chandler wobble, solid Earth tides, postglacial rebound, seismic free oscillations, and hydrology [21]. In addition to geophysics, they have been used to search for a dependence of gravity on a hypothetical preferred reference frame [22,23], or the violation of Lorentz invariance [24,25], as the Earth translates or rotates. In addition, gravimeters have been used to search for oscillations of the Earth excited by gravitational waves [26].

If there are many CDOs moving through the inner Solar System, it is possible that over the Solar System's lifetime a three body interaction (such as a close encounter of a binary system with the Earth) or some other mechanism could lead to the capture of a CDO in orbit around, *or through*, the Earth. For example, Neptune's moon Triton is thought to have been captured in this way [27]. Although capture might be rare, it could greatly aid the detection of what otherwise are probably very difficult to observe objects. As an alternative to relying on capture, one could search for unbound CDOs moving through the Earth; see, e.g., Ref. [28]. However, for our mass range, such events are likely extremely rare.

We assume that the unknown interactions between the CDO and Earth matter are small enough so that the CDO can move through the Earth with only modest dissipation. If so, this modest dissipation from dynamical friction [29,30] and/or additional weak nongravitational interactions could cause the orbit to slowly decay so that today

the CDO could be orbiting *inside* the Earth's inner core. We note that the CDO will move subsonically unless the radius of its orbit is nearly the radius of the Earth (or larger). Dynamical friction for subsonic motion in a gas could lead to an orbital decay time of order $(TM_\oplus)/m_D$ [29], where T is the orbital period (see below), M_\oplus is the mass of the Earth, and m_D is the mass of the CDO. For $m_D \approx 10^{-12}M_\oplus$, this decay time is of order 10^8 y.

An object moving in a circular orbit through an average density $\bar{\rho}$ will orbit with period T and frequency ν given by Kepler's third law,

$$\nu = \frac{1}{T} = \left(\frac{1}{3\pi} G\bar{\rho} \right)^{1/2}. \quad (1)$$

The density of the Earth $\rho(r)$ [31] is plotted in Fig. 1 along with the average density $\bar{\rho}(r)$ of matter interior to radius r . The orbital frequency ν varies from ≈ 0.3 mHz for small r to 0.2 mHz at the surface. Near the center of the Earth $\bar{\rho} \approx \rho_c = 13.1$ g/cm³ and is nearly constant [31]. For a constant density, the orbits are ellipses with the center of the ellipse coincident with the center of the Earth and the period is independent of r .

Gravimeters on the surface of the Earth could be sensitive to CDOs moving in the inner core by looking for very small periodic changes in the local acceleration from gravity (little g) with period near $T = 55$ min or frequencies near $\nu(\bar{\rho} = \rho_c) = \nu_0 = 0.305$ mHz (or somewhat smaller for larger radius orbits). In general, we do not know m_D or the radius of the orbit. However, we know the (approximate) orbital frequency ν_0 because we know the density profile inside the Earth.

As a first example, consider a gravimeter at the North Pole and a CDO that is oscillating along the Earth's rotation axis with time-dependent position $x(t) = a \cos(\omega t)$.

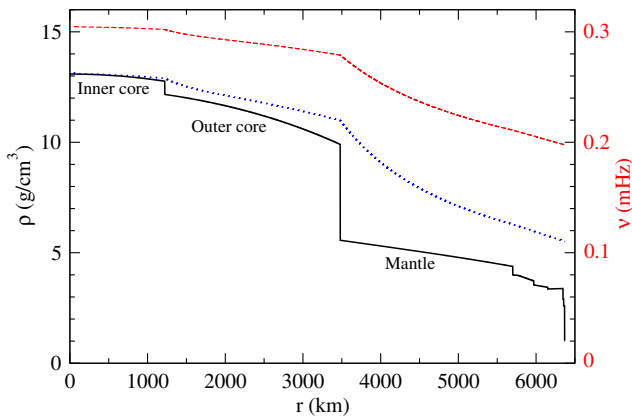


FIG. 1. Density of the Earth $\rho(r)$ versus radius r (solid black line) [31]. The dotted blue line shows the average density (of matter interior to r) $\bar{\rho}(r)$. Finally, the orbital frequency ν for a circular orbit inside the Earth of radius r is shown as the dashed red line using the right-hand scale.

Here, a is the amplitude of the motion and $\omega = 2\pi\nu_0$. The center of mass of the Earth will recoil so that its acceleration is $d^2X_\oplus(t)/dt^2 = \omega^2(m_D/M_\oplus)a \cos(\omega t)$. We assume $m_D \ll M_\oplus$. The gravimeter will have a time-dependent reading for two reasons. First, the meter is accelerating because it is on the (assumed rigid) Earth that is recoiling. Second, the gravitational acceleration due to the CDO will change with time as the distance between the CDO and the gravimeter changes. As we will see, both contributions are of order $(m_D a)/(M_\oplus R_\oplus)$ times g . Here the acceleration due to Earth's gravity is $g = GM_\oplus/R_\oplus^2$.

The gravitational acceleration g_D at the gravimeter from the CDO is

$$g_D = \frac{Gm_D}{[R_\oplus - a \cos(\omega t)]^2} \approx \frac{Gm_D}{R_\oplus^2} \left[1 + 2 \frac{a}{R_\oplus} \cos(\omega t) \right], \quad (2)$$

assuming $a \ll R_\oplus$. The time-dependent total gravimeter reading $\Delta g(t)$ is

$$\Delta g(t) \approx \left[\omega^2 a \frac{m_D}{M_\oplus} + 2 \frac{Gm_D a}{R_\oplus^3} \right] \cos(\omega t). \quad (3)$$

Using ω from Eq. (1) (with $\bar{\rho} \approx \rho_c$ given $a \ll R_\oplus$) and introducing the average density of the Earth $\bar{\rho}_\oplus = 3M_\oplus/(4\pi R_\oplus^3) \approx 5.51$ g/cm³, Eq. (3) can be written,

$$\frac{\Delta g(t)}{g} \approx \left(2 + \frac{\rho_c}{\bar{\rho}_\oplus} \right) \left(\frac{m_D a}{M_\oplus R_\oplus} \right) \cos(\omega t). \quad (4)$$

Thus, the gravimeter reading oscillates at frequency $\nu_0 = 0.305$ mHz with fractional amplitude (compared to g) of order $(m_D a)/(M_\oplus R_\oplus)$.

We now consider the more general case where the CDO is in a circular orbit of radius a ($\ll R_\oplus$) that is inclined by an angle Θ_I with respect to the plane of the equator. Let the gravimeter be located at latitude Θ_L . The time-dependent gravimeter reading is now [32]

$$\frac{\Delta g(t)}{g} = \left(2 + \frac{\rho_c}{\bar{\rho}_\oplus} \right) \left(\frac{m_D a}{M_\oplus R_\oplus} \right) \Delta(t) \quad (5)$$

with $\Delta(t) = \delta_1 \cos(\omega - \omega_\oplus)t + \delta_2 \cos(\omega + \omega_\oplus)t + \delta_3 \sin \omega t$. Here, $\delta_1 = \cos \Theta_L \cos^2 \Theta_I/2$, $\delta_2 = \cos \Theta_L \sin^2 \Theta_I/2$, and $\delta_3 = \sin \Theta_L \sin \Theta_I$. In addition to the original signal at angular frequency ω , there are now signals at the rotational sideband frequencies $\omega \pm \omega_\oplus$ with $\omega_\oplus = 2\pi/\text{day}$. This is because the gravimeter rotates with the Earth.

Equation (5) for a circular orbit has a very similar form to Eq. (4) for an extremely eccentric orbit. Therefore, we do not expect the gravimeter signal to depend strongly on the eccentricity of the orbit. Finally, the orientation of the orbit will slowly advance in time because the Earth's density is

not constant [32]. However, we do not expect this to significantly modify the gravimeter signal.

We now analyze gravimeter data. A number of superconducting gravimeters (SGs) have been deployed at various locations around the world. Data from these devices have been archived by the Global Geodynamics Project (1997–2015) and by the International Geodynamics and Earth Tide Service (2015–) [20,33]. The sensor self-noise of these instruments improved in 2009 when the manufacturer increased the mass of the levitated proof mass from 4 to 17.2 g [34]. At the Black Forest Observatory (BFO at 48.33°N, 8.33°E) in southwestern Germany, the first of these new SGs was installed, and because of its low noise level we will concentrate our analysis on data from that instrument. The analysis is complemented with the data from the SG in Canberra (CB at 35.32°S, 149.01°E).

We analyze about ten years of data from each instrument. The gravimeter data contain signals from numerous phenomena including tides, earthquakes, and atmospheric processes. The frequency band of interest here—0.2 to 0.3 mHz—is above the tides but overlaps with the lowest order seismic free oscillation. The largest signal in this band is from Newtonian attraction of variable air masses in the atmosphere above the sensor [21,35]. Since this is a well-known effect, all gravimeters are also equipped with a continuously recording barometer. For the simple model of a horizontally layered atmosphere over a rigid half-space, the admittance between a pressure perturbation and the resulting gravity perturbation is $\Delta g/\Delta p = -2\pi G/g = -4.27 \text{ nm s}^{-2}/\text{hPa}$. This admittance is reduced by two smaller but related effects that both have opposite sign to the Newtonian attraction effect. The indentation of the Earth’s crust by the barometric load leads to (1) an inertial downward acceleration and (2) a vertical motion of the gravimeter in a gradient field. Since we do not know the rigidity of the Earth’s crust at the site of the gravimeter and since we anticipate that the admittance also exhibits some frequency dependence [36], we estimate the gravity-pressure admittance with a one parameter least squares regression. We obtain empirical admittances of -3.0 and $-2.9 \text{ nm s}^{-2}/\text{hPa}$ for BFO and CB, respectively. To remove the atmosphere-induced signal, we use these admittances as scale factors and subtract the locally recorded barometric pressure from the raw gravity data. We find that in our frequency band the pressure correction is very efficient. In fact, the atmosphere accounts for 60% of the raw gravity signal, while other sources account for less than 40%.

How much the detection level depends on the chosen admittance has been addressed in the Supplemental Material [32]. As long as an admittance between -2.5 and $-4 \text{ nm s}^{-2}/\text{hPa}$ is used, the gravity spectral level, and hence, the CDO detection level in Figs. 2 and 3, changes by less than 5%.

Multi-year-long recordings cannot be analyzed without careful handling of artifacts in the data: times when the

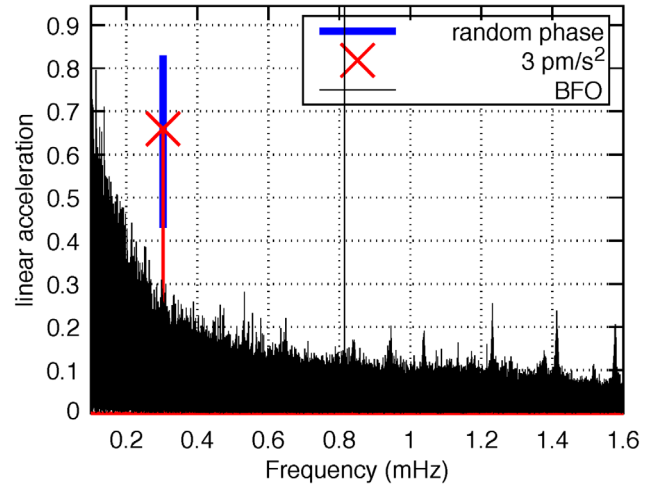


FIG. 2. Fourier amplitude spectrum of gravity residuals at station BFO versus frequency, solid black. The time series starts on July 20, 2011 and is 6.7 years long. The gravity data have been corrected for the atmospheric pressure with an admittance of $-3.0 \text{ nm s}^{-2}/\text{hPa}$. The red line with a cross shows calibration injections at a frequency of 0.303 mHz with an amplitude of 3 pm/s^2 and different phases shown by the blue band.

instrument behaved nonlinearly due to saturation from large quakes, operator interference (helium refills, cold head replacements, etc.), or other malfunctions. The gravity recordings are dominated by the tidal signal which can be well predicted [37]. So, we subtract from the data a synthetic tidal model for the stations that includes the effect of ocean loading. Subsequently, the residual signal is visually inspected, and we interactively flag large segments

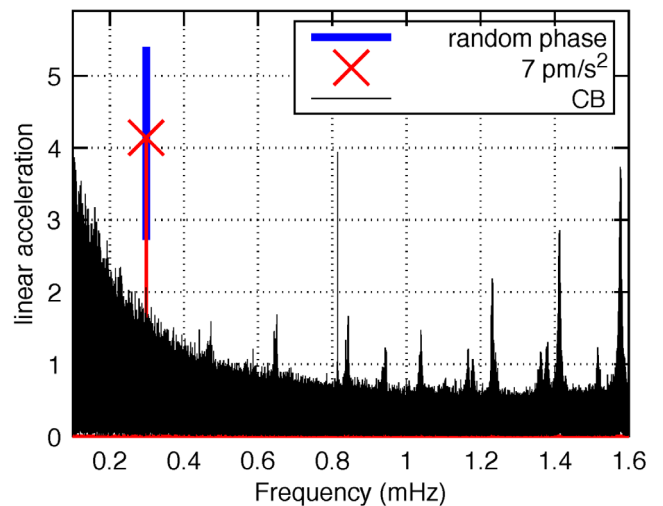


FIG. 3. Fourier amplitude spectrum of pressure-corrected gravity residuals at station CB similar to Fig. 2. The dataset starts on January 1, 2010 and is nine years long. The spectrum of one sinusoid at 0.3 mHz with the same data gaps and the same tapering as the gravity residuals is shown in red. Its amplitude is 7 pm/s^2 .

of bad data while short disturbances (< 1 h) are replaced by linear interpolation. We start with raw acceleration data sampled at 1 s intervals $\Delta g(t)$ [33] and after processing arrive at band-passed (7200–300 s) data sampled at 4 min intervals. The SG gravimeter data are calibrated by comparison against a colocated free-fall FG-5 absolute gravimeter in which a He-Ne laser and a rubidium clock provide atomic length and frequency standards, respectively. Since we are interested in the frequency band, which is also occupied by the lowest order seismic free oscillations, we have additionally flagged the hours and days following the largest quakes. These quakes are rare but would still lead to undesirable modal peaks in our frequency band. After this preprocessing of the data, we arrive at a time series with 3% flagged data. The flagged segments are zeroed before subsequent spectral analysis. The Canberra results are similar to the BFO results; however, the noise is about 2 times larger. Therefore, we focus on the BFO results.

In Figs. 2 and 3, we show Fourier amplitude spectra of the pressure-corrected and Hanning tapered gravity residuals for BFO and CB, respectively. A number of background signals are visible at both stations. A narrow, large amplitude spectral peak is seen near 0.8 mHz. This is the fundamental monopole ($\ell = 0$) free oscillation ${}_0S_0$ (or breathing mode) of the Earth. This mode has a high Q factor ($Q = 5500$) and can remain excited for several months after a large earthquake. Next to ${}_0S_0$, fundamental spheroidal free oscillation modes of the Earth (${}_0S_\ell$) with angular order from $\ell = 3$ to 9 are seen near 0.46, 0.64, 0.84, 1.03, 1.23, 1.41, and 1.57 mHz. These modes are excited by large quakes.

The $\ell = 2$ mode ${}_0S_2$ deserves special consideration because its frequency is very close to that expected for a CDO. Figure 4 shows this mode clearly excited by the large Tohoku earthquake. However, if we remove data for short periods after earthquakes, then the mode is not a significant background.

To detect a phase coherent monochromatic signal in the gravity residues, we use a Fourier amplitude spectrum of the full length dataset. The Fourier transform is optimal for this task because its basis functions are our target signal (matched filter). Furthermore, we can rely on the fact that the Fourier amplitude of the phase coherent signal increases with the record length N , while the Fourier amplitude of the incoherent background only increases with \sqrt{N} . Thus, the signal-to-noise ratio increases with the square root of the record length.

In Figs. 2 and 3, we have also included the spectrum of a harmonic signal of known time-domain amplitude and identical gap structure and tapering as the gravity residues. If we inject the harmonic into the gravity residues by adding the two signals in the time domain, we expect a peak in the spectrum at the frequency of the injected harmonic whose amplitude depends on whether the two signals

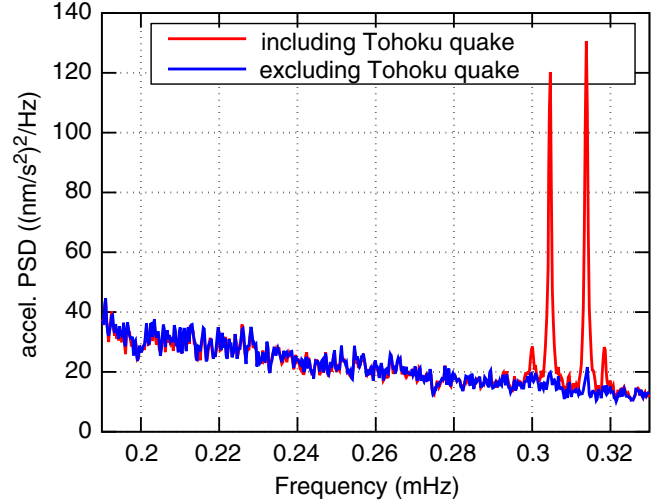


FIG. 4. Power spectral density of pressure-corrected gravity residuals at BFO for the CDO target frequency band. The longer dataset includes the magnitude Mw9.1 Tohoku event (March 11, 2011) and shows four out of the five singlets of the rotationally split fundamental spheroidal mode ${}_0S_2$. The longer dataset starts on October 1, 2010 and the shorter on July 20, 2011. They are 7.5 and 6.7 years long, respectively.

interfere constructively or destructively. Since the phase of the CDO signal is unknown, we varied the initial phase of the injected harmonic in steps of 15° and tracked the variation of the peak amplitude. This variation is indicated with the blue vertical bar. Thus, a 3 pm/s^2 harmonic gravity signal in the BFO gravity residues can show up in the Fourier amplitude spectrum with any value indicated by the blue bar.

Figure 2 shows that the total background at 0.3 mHz is significantly less than the 3 pm/s^2 calibration signal. Therefore, we set an upper limit at this frequency of

$$\Delta g(0.3 \text{ mHz}) < 3 \text{ pm/s}^2, \quad (6)$$

and a slightly larger value at 0.2 mHz. We now use this limit and Eq. (5) to set a limit on the product of CDO mass m_D and orbital radius a . The weakest limit is for CDO orbit inclination angle Θ_I that minimizes $F(\Theta_L)$ for a gravimeter at latitude Θ_L ,

$$F(\Theta_L) = \min_{\Theta_I}(\max[\delta_1, \delta_2, \delta_3]). \quad (7)$$

For the Black Forest Observatory at $\Theta_L = 48.33^\circ$, we have $F(48.33^\circ) \approx 0.555$. This occurs for $\Theta_I \approx 48^\circ$. Using Eqs. (5) and (7), we have $(m_D a)/(M_\oplus R_\oplus) < \Delta g(0.3 \text{ mHz})/[g(2 + [(\rho_c)/(\bar{\rho})])F(48.33^\circ)]$. Or using Eq. (6), our final limit is

$$\frac{m_D a}{M_\oplus R_\oplus} < \frac{3 \text{ pm/s}^2}{9.8 \text{ m/s}^2 \times 4.38 \times 0.555} = 1.2 \times 10^{-13}. \quad (8)$$

This equation is our main result. We are able to set a very strict limit because the gravimeter is very sensitive.

In general, we do not know the orbital radius a . For reference, let us consider $a \approx 0.1R_{\oplus}$. Our limit is now

$$m_D < 1.2 \times 10^{-12} M_{\oplus} = 4 \times 10^{-18} M_{\odot} = 7 \times 10^{12} \text{ kg.} \quad (9)$$

Of course, if a is much smaller than $0.1R_{\oplus}$, the limit on m_D becomes larger, but this equation provides an order of magnitude expectation. Equation (9) is over 10^6 times smaller than the $10^{-11} M_{\odot}$ lowest mass probed by microlensing [9].

Since we do not observe any objects, we can set a limit on the probability of capture of a CDO in a collision with Earth. If all of dark matter is made of CDOs (of a given mass) and CDOs orbit for a long time inside the Earth, then the probability of capture must be less than $\approx 10^{-3}$ for $m_D = 10^{-18} M_{\odot}$ to less than $\approx 10^{-1}$ for $m_D = 10^{-16} M_{\odot}$. Please see the Supplemental Material for details [32].

One can search for CDOs in other Solar System bodies. The Moon has no atmosphere and therefore little noise from atmospheric fluctuations. The Lunar Surface Gravimeter was deployed on the moon during the Apollo 17 mission [38,39]. Unfortunately, this instrument had a design flaw. The space-based gravitational wave detector LISA should be sensitive to GW radiation from CDOs moving in the Sun or Jupiter, although a detection will likely require a significantly more massive object [40].

In conclusion, dark matter could be composed of CDOs. These objects may interact very weakly with normal matter and could move freely inside the Earth. We have searched superconducting gravimeter data and ruled out CDOs moving in the Earth unless their masses m_D and or orbital radii a are very small so that $m_D a < 1.2 \times 10^{-13} M_{\oplus} R_{\oplus}$. Here, M_{\oplus} and R_{\oplus} are the mass and radius of the Earth, respectively.

We acknowledge helpful discussions with Tamara Bogdanovic, Matt Caplan, Nicole Kinsman, Rafael Lang, Cole Miller, Maria Alessandra Papa, and Walter Zürn. C. J. H. thanks the Max Planck Institute for Gravitational Physics in Hannover and the KITP in Santa Barbara for their hospitality. C. J. H. is supported in part by the U.S. Department of Energy Grants No. DE-FG02-87ER40365 and No. DE-SC0018083. The SG at BFO was funded jointly by the Deutsche Forschungsgemeinschaft (DFG, German Research Foundation) – Project No. 66823308, the Karlsruhe Institute of Technology (KIT) and the Stuttgart University. We gratefully acknowledge the work of the operators of the superconducting gravimeters: Harry McQueen and Tadahiro Sato from the National Astronomical Observatory, Mizusawa for the Canberra station, and Thomas Forbriger and Peter Duffner from the Karlsruhe Institute of Technology for the Black Forest

Observatory. We thank the data centers for archiving and freely distributing the gravimetric data and Th. Forbriger for porting the ETERNA software package for tidal predictions to UNIX [41].

*horowitz@indiana.edu

†widmer@gis.uni-stuttgart.de

- [1] F. Kühnel and K. Freese, *Phys. Rev. D* **95**, 083508 (2017).
- [2] S. L. Liebling and C. Palenzuela, *Living Rev. Relativity* **20**, 5 (2017).
- [3] D. M. Grabowska, T. Melia, and S. Rajendran, *Phys. Rev. D* **98**, 115020 (2018).
- [4] M. I. Gresham, H. K. Lou, and K. M. Zurek, *Phys. Rev. D* **97**, 036003 (2018).
- [5] G. F. Giudice, M. McCullough, and A. Urbano, *J. Cosmol. Astropart. Phys.* **10** (2016) 001.
- [6] T. Bringmann, P. Scott, and Y. Akrami, *Phys. Rev. D* **85**, 125027 (2012).
- [7] F. Yang, M. Su, and Y. Zhao, [arXiv:1712.01724](https://arxiv.org/abs/1712.01724).
- [8] D. M. Jacobs, G. D. Starkman, and B. W. Lynn, *Mon Not. R. Astron. Soc.* **450**, 3418 (2015).
- [9] H. Niikura, M. Takada, N. Yasuda, R. H. Lupton, T. Sumi *et al.*, *Nat. Astron.* **3**, 524 (2019).
- [10] C. Alcock, R. A. Allsman, T. S. Axelrod, D. P. Bennett, K. H. Cook *et al.* (MACHO Collaboration), *Phys. Rev. Lett.* **74**, 2867 (1995).
- [11] C. Alcock, R. A. Allsman, T. S. Axelrod, D. P. Bennett, K. H. Cook *et al.* (MACHO Collaboration), *Astrophys. J.* **542**, 281 (2000).
- [12] P. Tisserand *et al.* (EROS-2 Collaboration), *Astron. Astrophys.* **469**, 387 (2007).
- [13] B. Paczynski, *Astrophys. J.* **304**, 1 (1986).
- [14] V. Cardoso and P. Pani, *Living Rev. Relativity* **22**, 4 (2019).
- [15] B. P. Abbott, R. Abbott, T. D. Abbott, F. Acernese, K. Ackley, C. Adams, T. Adams, P. Addesso, R. X. Adhikari, V. B. Adya *et al.* (LIGO Scientific Collaboration and Virgo Collaboration), *Phys. Rev. Lett.* **121**, 231103 (2018).
- [16] C. J. Horowitz and S. Reddy, *Phys. Rev. Lett.* **122**, 071102 (2019).
- [17] C. J. Horowitz, M. A. Papa, and S. Reddy, *Phys. Lett. B* **800**, 135072 (2020).
- [18] A. Katz, J. Kopp, S. Sibiryakov, and W. Xue, *J. Cosmol. Astropart. Phys.* **12** (2018) 005.
- [19] J. M. Goodkind, *Rev. Sci. Instrum.* **70**, 4131 (1999).
- [20] C. Voigt, C. Förste, H. Wziontek, D. Crossley, B. Meurers, V. Palinkas, J. Hinderer, J.-P. Boy, J.-P. Barriot, and H. Sun, *Report on the Data Base of the International Geodynamics and Earth Tide Service (IGETS), GFZ German Research Centre for Geosciences, 2016*, https://doi.org/10.2312/GFZ_b103-16087.
- [21] J. Hinderer, D. Crossley, and R. Warburton, *Treatise on Geophysics*, edited by T. Herring and G. Schubert (Elsevier, New York, 2007), Vol. 3, p. 65.
- [22] C. M. Will and K. Nordtvedt, *Astrophys. J.* **177**, 757 (1972).
- [23] R. J. Warburton and J. M. Goodkind, *Astrophys. J.* **208**, 881 (1976).

- [24] N. A. Flowers, C. Goodge, and J. D. Tasson, *Phys. Rev. Lett.* **119**, 201101 (2017).
- [25] C.-G. Shao, Y.-F. Chen, R. Sun, L.-S. Cao, M.-K. Zhou, Z.-K. Hu, C. Yu, and H. Müller, *Phys. Rev. D* **97**, 024019 (2018).
- [26] M. Coughlin and J. Harms, *Phys. Rev. D* **90**, 042005 (2014).
- [27] C. B. Agnor and D. P. Hamilton, *Nature (London)* **441**, 192 (2006).
- [28] J. S. Sidhu and G. Starkman, *Phys. Rev. D* **100**, 123008 (2019).
- [29] E. C. Ostriker, *Astrophys. J.* **513**, 252 (1999).
- [30] W.-T. Kim, *Astrophys. J.* **725**, 1069 (2010).
- [31] A. M. Dziewonski and D. L. Anderson, *Phys. Earth Planet. Inter.* **25**, 297 (1981).
- [32] See Supplemental Material at <http://link.aps.org/supplemental/10.1103/PhysRevLett.124.051102> for further details of the data analysis and the CDO orbits.
- [33] J.-P. Boy, Superconducting Gravimeter Data-Level 3, GFZ Data Services, <http://isdg.gfz-potsdam.de/igets-data-base/>.
- [34] S. Rosat and J. Hinderer, *Bull. Seismol. Soc. Am.* **101**, 1233 (2011).
- [35] W. Zürn and E. Wielandt, *Geophys. J. Int.* **168**, 647 (2007).
- [36] R. J. Warburton and J. M. Goodkind, *Geophys. J. Int.* **48**, 281 (1977).
- [37] H.-G. Wenzel, *Bull. Inf. Marees Terrestres* **124**, 9425 (1996), <http://www.bim-icet.org>.
- [38] J. J. Giganti, J. V. Larson, J. P. Richard, R. L. Tobias, and J. Weber, Lunar Surface Gravimeter Experiment Final Report, University of Maryland, Department of Physics and Astronomy, 1977.
- [39] T. Kawamura, N. Kobayashi, S. Tanaka, and P. Lognonné, *J. Geophys. Res. Planet* **120**, 343 (2015).
- [40] T. Robson, N. Cornish, and C. Liu, *Classical Quantum Gravity* **36**, 105011 (2019).
- [41] T. Forbriger, <https://git.scc.kit.edu/ToE/Eterna>, 2018.